**UtilitasMathematica**

**ISSN 0315-3681 Volume 122, 2025**

# Enhanced Converter Control using PR Controller in Electric Springs

**P.Srinivasarao[1], M.R.Mohamed[1,*], K.K. Deepika[2], D.J K Kishore[3], A. Anjaneyulu[4]**

[1]Faculty of Electrical & Electronics Engineering Tech., Universiti Malaysia Pahang Al-Sultan Abdullah, Pekan, Malaysia.

[2]Department of Electrical & Electronics Engineering, VIGNAN's Institute of Information Technology, Vishakapatnam, India

[3]Department of Electrical & Electronics Engineering, Sri Vasavi Engineering College, Tadepalligudem, Andhra Pradesh, India

[4]Department of Electrical & Electronics Engineering, Sasi Institute of Technology & Engineering, Tadepalligudem, Andhra Pradesh, India

*Corresponding Author: rusllim@umpsa.edu.my

***Abstract*— Electric Spring is the recent paradigm in demand-side management to control the load demand following the generation. This paper details a diagnostic approach to the design of a Proportional Resonant (PR) controller for a single-phase grid-connected system with an Electric Spring (ES) with Back-to-Back Converter. Design is ensured using bode diagrams for various PR controller parameters. Also, the design of the DC-link voltage control loop is detailed. Fourier analysis is demonstrated to measure ripple content in a grid. Simulation results of Electric Spring with PR controller confirm the ability of ES to track reference power for fixed and variations in reference power, and dynamic load changes.**

**Keywords—Electric Springs, Proportional Resonant Controller, critical load, back-to-back converter.**

## I. INTRODUCTION

Electric spring was conceptualized in [1] and demonstrated to be effective in regulating the mains voltage despite the fluctuation initiated by the erratic nature of Renewable Energy Sources (RES). It was practically tested for both voltage support and suppression. It was also tested for shaping load demand (of about 2.5 kW) to follow the fluctuating wind power [2].

Electric springs in demand response technology have been widely used for mitigation of voltage and frequency fluctuations [3][4], and reduction of power imbalance [5][6]. ES has been demonstrated to track the variations in reference power [7]. When the reference power is surplus than the requirement of critical and non-critical loads, it is necessary to modify the ES with existing full bridge inverter configuration to feed the available surplus power to main grid. DC power side of ES must be interfaced with the AC grid. It is essential to include energy storage technology in the power converter to meet the difference in power between the two sides. Electric springs with Back-to-Back (ES-B2B) converter con-figuration [8][9] as illustrated in Fig. 1.

## II. CONTROL SCHEME OF ELECTRIC SPRINGS

For efficient power flow between ES and grid it is crucial to control the DC link voltage to be constant. This can be well-explained using two cases:

*A.* When the reference power is surplus than the requirement of critical and non-critical loads, ES transfers the surplus power to the grid through the DC link and converter circuit. Else, if the DC link voltage is less than the reference value, some amount of power is utilized to charge the DC link capacitor and the remaining is fed to the grid. Consequently, power fed to the grid is reduced.

B. During voltage fluctuations, the DC supply required for the inductive/capacitive mode of operation of ES is obtained from the DC link capacitor. So, the DC capacitor discharges to maintain its voltage at a fixed voltage. It takes power from grid through a rectifier circuit.

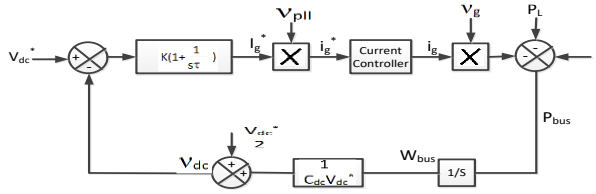


**Fig. 2.** DC link Voltage Control Loop with Current controller

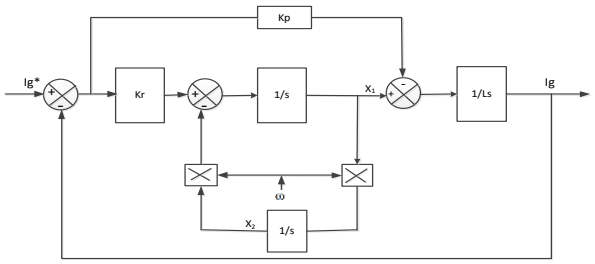


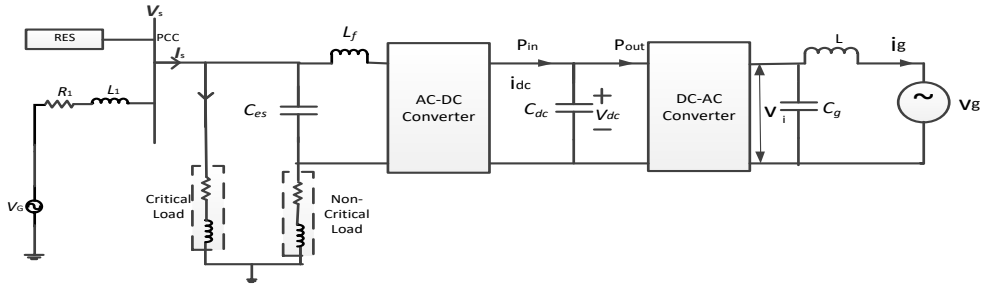


**Fig. 1.** Schematic diagram of ES with power flow across DC bus

At fundamental frequency, magnitude-frequency response of the system is zero and is expressed as[14][15]:

$$20\log\left|\left(\frac{2K_r\omega_b(j\omega_c)}{-{\omega_c}^2+2\omega_b(j\omega_c)+{\omega_1}^2}\right)\frac{1}{j\omega_c L}\right| = 0 \quad (4)$$

As $\omega_c > \omega_1$, by successive approximations Eq. (4) becomes:

$$20\log\left|\frac{K_P}{j\omega_c L}\right| = 0 \quad (5)$$

$$K_P = |j\omega_c L| \quad (6)$$

$$\frac{{i_g}^* - i_g}{{i_g}^*} = 1 - \frac{G(s)}{1+G(s)} \quad (7)$$

At fundamental frequency, steady-state error in injected grid current ($i_g$) is considered as η and is expressed as:

$$\eta = \frac{{i_g}^* - i_g}{{i_g}^*} \quad (8)$$

**Fig. 3.** Overall scheme for control of injected current

To realize an AC compensator with zero phase and magnitude error equivalent to DC compensator (transfer function $H_{DC}(s)$) is given by [10]-[13] :

$$H_{AC}(s) = H_{DC}(s)\left(\frac{s^2+{\omega_1}^2}{2s}\right) \quad (1)$$

When given as input to a PI controller, it is:

$$H_{AC}(s) = K_P + \frac{2K_i s}{s^2+{\omega_1}^2} \quad (2)$$

where $K_P$: Proportional gain, $K_{r:}$ Resonant gain, $\omega_{1:}$ is fundamental frequency. High pass filter is modified to give a finite gain and is given by Eq. (3), where $\omega_b$ as the lower breakpoint frequency and $\omega_c$ is the cut-off frequency.

$$H_{AC}(s) = K_P + \frac{2K_r\omega_b s}{s^2+2\omega_b s+{\omega_1}^2} \quad (3)$$

$$Then, \eta = \frac{1}{1+G(s)} \quad (9)$$

So, at $\omega_1$, open loop transfer function and phase-response of the PR controller will be given by (11) and (13) respectively as:

$$|G(j\omega_1)| = \frac{1}{\eta} - 1 \quad (10)$$

$$PR(s) = \frac{s^2+2\omega_b s\left(1+\frac{K_r}{K_P}\right)+{\omega_1}^2}{s^2+2\omega_b s+\omega^2} \quad (11)$$

$$\Phi(\omega) = K_p + \frac{2K_r\omega_b s}{s^2+2\omega_b s+{\omega_1}^2} \quad (12)$$

$$\Phi(\omega) = \mathrm{Tan}^{-1}\left(\frac{2\omega_b\omega\left(1+\frac{K_r}{K_P}\right)}{{\omega_1}^2-{\omega_c}^2}\right) - \mathrm{Tan}^{-1}\left(\frac{2\omega_b\omega}{{\omega_1}^2-{\omega_c}^2}\right) \quad (13)$$

For stability, $\Phi(\omega_c) > -\Phi$

$$\text{Or, } \{\text{Tan}^{-1}\left(\frac{2\omega_b\omega_c\left(1+\frac{K_r}{K_P}\right)}{{\omega_1}^2-{\omega_c}^2}\right)-\text{Tan}^{-1}\left(\frac{2\omega_b\omega_c}{{\omega_1}^2-{\omega_c}^2}\right)\}> -\Phi \quad (14)$$

$$|L(\omega_1|G(j\omega_1)|-\omega_C| \leq K_r \leq \left|K_P\left\{\left(\frac{{\omega_1}^2-{\omega_c}^2}{2\omega_b\omega_c}\right)\text{Tan}\left\{\text{Tan}^{-1}\left(\frac{2\omega_b\omega_c}{{\omega_1}^2{\omega_c}^2}\right)-\Phi\right\}-1\right\}\right| \quad (15)$$

According to Eq. (15) minimum and maximum threshold limits of PR controller can be defined by Eq. (16) and (17) respectively:

$$K_{r\_min.}=|L(\omega_1|G(j\omega_1)|-\omega_C| \quad (16)$$

$$K_{r\_max.}=\left|K_P\left\{\left(\frac{{\omega_1}^2-{\omega_c}^2}{2\omega_b\omega_c}\right)tan\left\{\text{tan}^{-1}\left(\frac{2\omega_b\omega_c}{{\omega_1}^2{\omega_c}^2}\right)-\Phi\right\}-1\right\}\right| \quad (17)$$

Evaluating (16) and (17) yields to: $K_{r\_min.}$ = 149 and $K_{r\_max.}$ = 2000.

## III. Simulation Results

### A. *Design of PR controller*

System parameters taken for simulation are given in Table 1. Cut-off frequency is always less than one-tenth of the switching frequency [10], thus cut-off frequency is selected to be 1000Hz.

**Table 1.** System Parameters

| Name | Value |
|---|---|
| Switching Frequency | 10 KHz |
| Fundamental frequency | 50 Hz |
| Grid Phase voltage | 230V |
| L filter inductor | 6 mH |

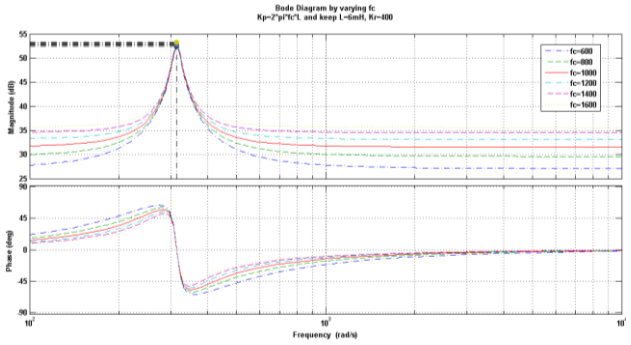

(a)

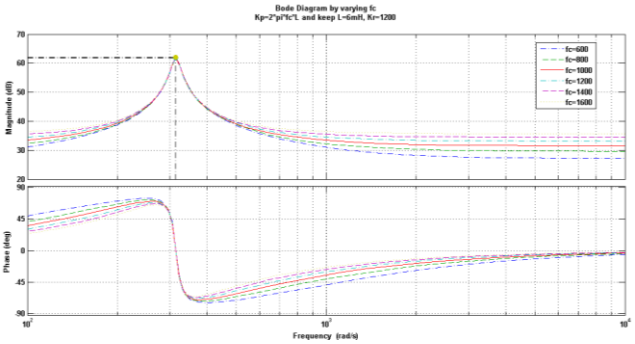

(b)

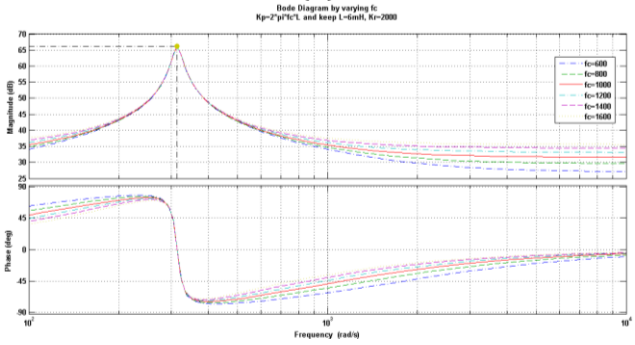

(c)

**Fig. 4.** Open-loop performance of PR controller at various cutoff frequencies, $K_r$

An increase in cutoff frequency widens the bandwidth, as illustrated in Fig. 4(a), Fig. 4(b) and Fig. 4(c). It can be increased further with the increase in $K_r$ value from 400 to 2000. For a particular resonant term, the peak amplitude remains the same irrespective of the changes in cut-off frequency, whereas this magnitude increases with increase in $K_r$ value. For $K_r$= 400, peak amplitude is around 53db and it is increased to about 66 db for $K_r$= 2000. The same is illustrated in Fig. 5(a), Fig. 5(b) and Fig. 5(c).

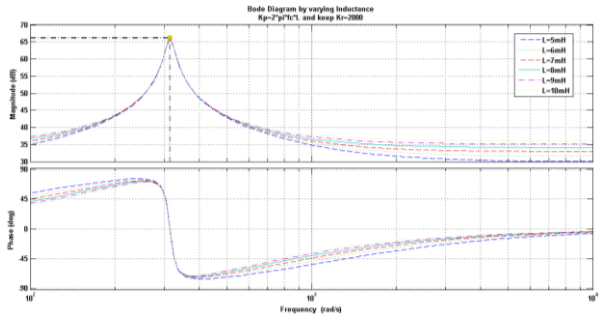

(a)

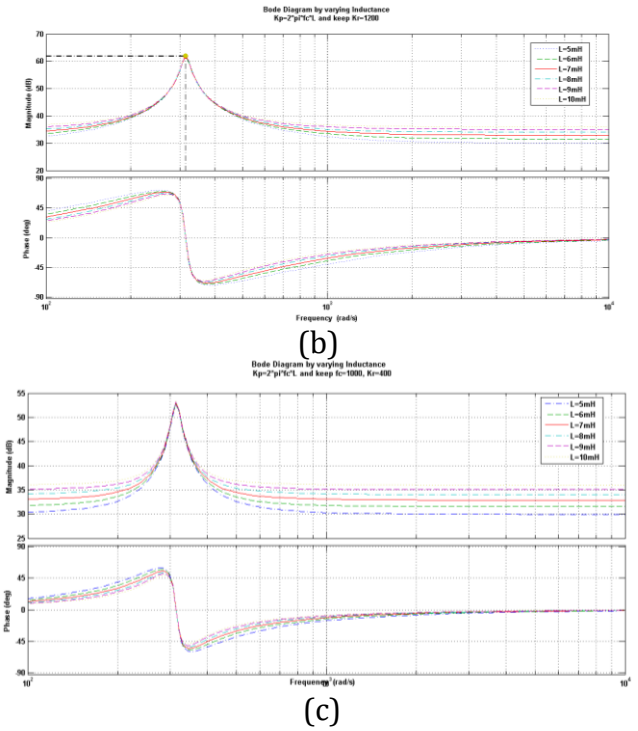


**Fig. 5.** Open-loop performance of PR controller at various $K_p$ , L values

Fig. 6 shows the perfect tracking of the injected grid current in 4ms by the PR controller to the variations in the reference current at t=0.1 sec.

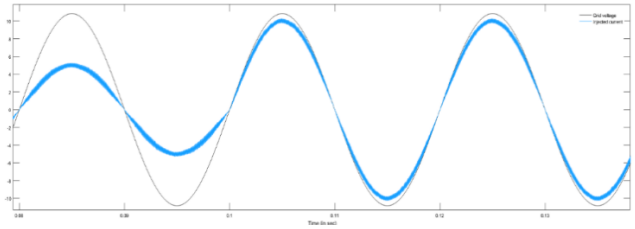

**Fig. 6.** Grid voltage (scaled down) and injected current when reference current is increased from 5 A to 10A at t=0.1 sec.

The current tracking ability by the designed PR controller is compared with PI controller. PR controller demonstrates a superior performance with reduced ripple in converter current and faster tracking of grid current as demonstrated with FFT Analysis in Fig. 8(a), (b). %THD is 4.54 with PI controller and it is reduced to 4.16 with PR controller.

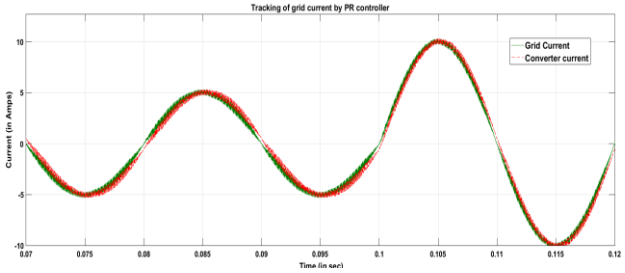


**Fig. 7.** Current tracking by PR controller for step change in grid current

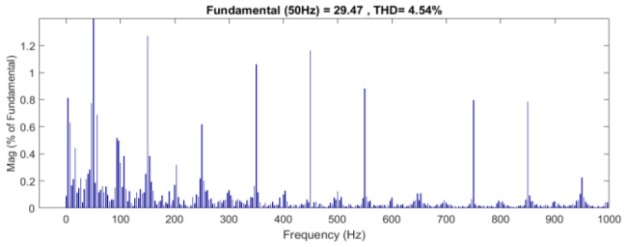


**(a) PI controller**

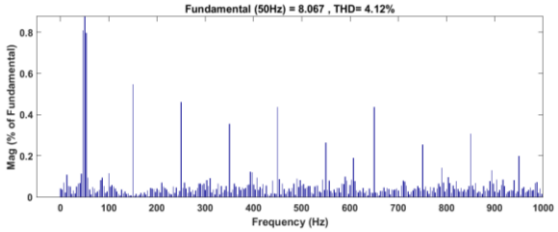


**(b) PR controller**

**Fig. 8.** FFT Analysis of Grid current with PI, PR controllers

*B. Design of DC link voltage control loop*

**Table 2.** Parameters of DC link voltage control loop

| Parameter | Value |
|---|---|
| Maximum load variation, $V_{dc(\max)}$ | 200 Watts |
| Filter delay time, $T_r$ | 0.02 sec |
| DC-link capacitor voltage, $C_{dc}$ | 400 Volts |
| Voltage variation in the DC-link capacitor, $\Delta V_{dc(\max)}$ | 0.01 Volts |
| DC link capacitance, $C_{dc}$ | 4700 mF |
| Filter inductance, $L_g$ | 2mH |
| Filter capacitance, $C_g$ | 20 µF |

*C. System performance*

In this case, power tracking operation of ES with back to back converter under steady state and

dynamic conditions is analyzed. Reference power of 8 KW is given to ES system.

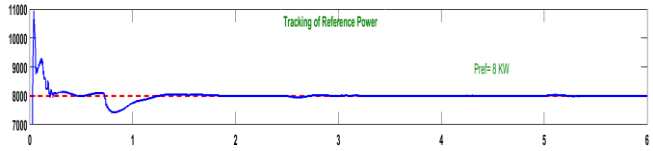


**Fig. 9.** Performance of ES for constant reference power

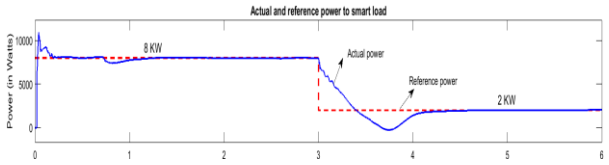


**Fig. 10.** Performance of ES for change in reference power from 8 to 2 KW

Critical load 2 of (16Ω + 0.2 mH) is connected in parallel to the existing critical load 1 of the same value. Load 2 is connected from 2 to 4 seconds. Fig. 11 highlights that ES seamlessly tracks the reference power under dynamic load changes. Similarly performance of ES for change in Non-critical loads is demonstrated in Fig. 12.

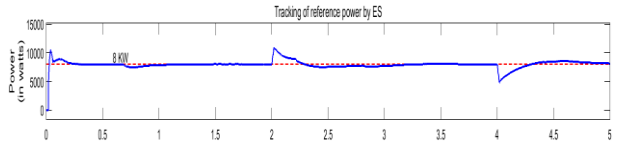


**Fig. 11.** Performance of ES for change in critical load

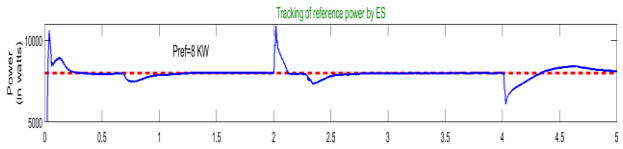


**Fig. 12.** Performance of ES for change in Non-critical load

## IV. Conclusion

This paper presents a detailed diagnostic approach to the design of a Proportional resonant controller for a single-phase grid connected system with Electric Spring. Broad studies in design are analyzed using bode diagrams for various PR controller parameters. It was demonstrated that ripple content in grid current is reduced with PR controller than a conventional PI controller. Simulation results of Electric Spring with PR controller have indicated effectiveness to track reference power for fixed and variations in reference power, and dynamic load changes.

## ACKNOWLEDGEMENT

This work is supported by Universiti Malaysia Pahang Al-Sultan Abdulaah (UMPSA) through grant no. (PGRS230350) , and Mr. Palla Srinivasarao is working under UMPSA's Doctoral Research Scheme (DRS).

## References

[1] D. Westermann and A. John, "Demand matching wind power generation with wide-area measurement and demand-side management," IEEE Trans. Energy Conversion, vol. 22, no. 1, pp. 145–149, 2007.

[2] P. Palensky and D. Dietrich, "Demand side management: Demand response, intelligent energy systems, and smart loads," IEEE Trans. Ind.Informatics, vol. 7, no. 3, pp. 381–388, 2011.

[3] C. K. Lee, S. N. Li, and S. Y. R. Hui, "A design methodology for smart LED lighting systems powered by weakly regulated renewable power girds," IEEE Trans. Smart Grid, vol. 2, no. 3, pp. 548–554, Sep. 2011.

[4] S. Y. Hui, C. K. Lee and F. F. Wu, "Electric Springs—A New Smart Grid Technology," in IEEE Transactions on Smart Grid, vol. 3, no. 3, pp. 1552-1561, Sept. 2012, doi:10.1109/TSG.2012.2200701.

[5] Lee CK, Shu YH. Reduction of energy storage requirements in future smart grid using electric springs. IEEE Transactions on Smart Grid 2013; 4(3):1282–1288.

[6] Yan S, Lee CK, Yang T, Mok KT, Tan SC, Chaudhuri B, Shu YH. Extending the operating range of electric spring using back-to-back converter: Hardware implementation and control. IEEE

Transactions on Power Electronics 2017; 32(7):5171–5179.

[7] Yan, S., Lee, C.-K., Yang, T., Mok, K.-T., Tan, S.-C., Chaudhuri, B., & Hui, S. Y. R. (2017). Extending the Operating Range of Electric Spring Using Back-To-Back Converter: Hardware Implementation and Control. IEEE Transactions on Power Electronics, 32(7), 5171–5179.

[8] ZHENG, Y., ZHANG, C., HILL, D.J. et al. Consensus control of electric spring using back-to-back converter for voltage regulation with ultra-high renewable penetration. J. Mod. Power Syst. Clean Energy 5, 897–907 (2017). https://doi.org/10.1007/s40565-017-0338-4.

[9] Deepika.K.K, Kumar, J. & Varma, Pinni & Sura, Srinivasa & Sankar, R.. (2022). Design of Back-to-Back Converter Interface for Electric Spring in a Distribution System. Frontiers in Energy Research. 10. 765899. 10.3389/fenrg.2022.765899.

[10] Wei, Y., Zhao, C. & Duan, Y. Design of Single-Phase Electrical Spring Based on PR Controller and Critical Load Current Feedback. *J. Electr. Eng. Technol.* **17**, 3317–3328 (2022). https://doi.org/10.1007/s42835-022-01190-4

[11] D. Ilie-Ablachim, G. C. Pătru, I.-M. Florea, and D. Rosner, "Monitoring device for culture substrate growth parameters for precision agriculture: Acronym: MoniSen," in 2016 15th RoEduNet Conference: Networking in Education and Research, IEEE, 2016, pp. 1–7.

[12] I. Ahmed, M. Rehan, A. Basit, and K.-S. Hong, "Greenhouse gases emission reduction for electric power generation sector by efficient dispatching of thermal plants integrated with renewable systems," Sci. Rep., vol. 12, no. 1, p. 12380, 2022.

[13] E. C. Malz, V. Verendel, and S. Gros, "Computing the power profiles for an Airborne Wind Energy system based on large-scale wind data," Renew. Energy, vol. 162, pp. 766–778, 2020.

[14] J. Zha, J. Wu, and D. Zhao, "Effects of land use and cover change on the near-surface wind speed over China in the last 30 years," Prog. Phys. Geogr., vol. 41, no. 1, pp. 46–67, 2017.

[15] N. Aries, S. M. Boudia, and H. Ounis, "Deep assessment of wind speed distribution models: A case study of four sites in Algeria," Energy Convers. Manag., vol. 155, pp. 78–90, 2018.